

NANO EXPRESS

Open Access



CMOS-Compatible Fabrication for Photonic Crystal-Based Nanofluidic Structure

Wang Peng^{1,2,3,5}, Youping Chen¹, Wu Ai¹, Dailin Zhang^{1*}, Han Song⁴, Hui Xiong¹ and Pengcheng Huang¹

Abstract

Photonic crystal (PC)-based devices have been widely used since 1990s, while PC has just stepped into the research area of nanofluidic. In this paper, photonic crystal had been used as a complementary metal oxide semiconductors (CMOS) compatible part to create a nanofluidic structure. A nanofluidic structure prototype had been fabricated with CMOS-compatible techniques. The nanofluidic channels were sealed by direct bonding polydimethylsiloxane (PDMS) and the periodic gratings on photonic crystal structure. The PC was fabricated on a 4-in. Si wafer with Si_3N_4 as the guided mode layer and SiO_2 film as substrate layer. The higher order mode resonance wavelength of PC-based nanofluidic structure had been selected, which can confine the enhanced electrical field located inside the nanochannel area. A design flow chart was used to guide the fabrication process. By optimizing the fabrication device parameters, the periodic grating of PC-based nanofluidic structure had a high-fidelity profile with fill factor at 0.5. The enhanced electric field was optimized and located within the channel area, and it can be used for PC-based nanofluidic applications with high performance.

Keywords: Photonic crystal, PC-based nanofluidic structure, CMOS-compatible process, Periodical Si_3N_4 gratings

Background

Photonic crystal (PC) is defined as a relatively high refractive index layer of modulated periodic structure, and it is surrounded by two relatively low refractive index materials. When a collimated and polarized white light projects on the surface of the periodic structure, the PC can interact strongly with the specific optical wavelength, and the electric field of PC will be redistributed. Then, the specific wavelength is reflected back with a particular angle according to the light's incident direction, while the remained wavelengths light transmit through the PC structure. The reflected optical wavelength is regarded as optical resonance wavelength, and the electric field of PC gratings can be enhanced many times than the initial incident light. Since Yablonoitch proposed the concept of photonic crystal [1], PC have been used extensively in various fields, including PC-based waveguide [2], fiber [3], back reflector [4], and light-emitting diode [5].

With the rapid development of life science, the methods for gene detection, protein-binding analysis, small molecules, and DNA detection are urgently needed. PC-based biosensors are studied and fabricated widely. The principle for PC-based biosensors is the interaction between the liquid sample and the enhanced electric field of PC. Basically, there are two kinds of PC-based detection methods: label-free detection [6, 7] and fluorescence-enhanced detection [8–10]. However, all the PC-related devices rely on the enhanced electrical field magnitude on the surface of the PC gratings, which is known as evanescent field. The functional range of the evanescent field is under 300 nm from the PC surface [11], which means that the tremendous space of the PC-based bulk device cannot make a contribution to the detection result. Moreover, for PC-based chemical, biological, and medical applications, the analytes are either required to flow through optical sensor or bind to the surface of PC gratings by diffusion [12, 13] so as to use the evanescent field on the PC surface. With traditional bulk sensors, it may take several hours for the analytes to reach the surface of optical flow sensor due to the laminar flow [14, 15], especially in low concentration detection [16, 17]. Thus, the PC-based bulk sensors that require large volume of analytes and need a

* Correspondence: mnizhang@mail.hust.edu.cn

¹School of Mechanical Science and Engineering, Huazhong University of Science and Technology, Wuhan 430074, China

Full list of author information is available at the end of the article

long diffusion time may not be adaptable for future detection among proteins, genes, and small molecules. However, PC-based nanofluidic sensors paved a new way for efficient and high-performance detection [18–20]. The nanofluidic channel can guarantee the detection area be confined around the evanescent region of PC structure, which can improve the sensor’s sensitivity and reduce sample volume. Also, due to the large surface to volume ratio, the analytes in the nanochannels can flow to the channel walls easily.

In this paper, a novel PC-based nanofluidic structure has been designed and fabricated with CMOS-compatible process [21]. PC-based nanofluidic structure is an important CMOS-compatible part, and it can be used to realize the lab on a Chip concept for parallel and high throughput applications. The PC-based nanofluidic structure was fabricated on a 4-in. Si wafer, with Si₃N₄ as the high refractive index layer and SiO₂ as relatively low refractive index substrate. A PDMS stamp was used to directly seal the PC gratings and create the nanochannels. The PC gratings were patterned by PMMA with e-beam lithography, and then the grating patterns were transferred to a thin chrome layer. The chrome was used as hard mask to transfer the grating pattern precisely to the Si₃N₄ film. All the related parameters had been analyzed and calculated during the fabrication processes.

Methods

Principle of PC-Based Nanofluidic Structure

The proposed nanofluidic sensor structure is shown in Fig. 1a: the PC structure is configured by periodical Si₃N₄ layer as guided layer and a flat SiO₂ layer on top of Si wafer as substrate, and PDMS is used as cladding layer to seal the PC gratings. As shown in Fig. 1b, the inlet and outlet of the nanofluidic structure were drilled from the back side of Si wafer. With this structure, the resonance wavelength energy can be largely coupled into the guided layer and reduce the leaked energy around

resonance wavelength of the PC. The Si₃N₄ layer thickness is d₀, and the grating depth is d_g. The thickness of SiO₂ layer is d_{sub}, and it was used as relatively low refractive index for PC. As discussed in [22], there were several parameters influence the resonance wavelength of PC-based nanofluidic structure. The subwavelength pitch and the remained thickness of Si₃N₄ determine the peak wavelength position of the PC, while the grating depth d_g can be used to tune the PC bandwidth. The resonance wavelength generated when the collimated and polarized incident light source matches with phase-matching condition [23], as shown in Eq. (1):

$$\frac{2\pi}{\lambda} n_{eff} = \frac{2\pi}{\lambda} n_c \sin\theta \pm m \left(\frac{2\pi}{\Lambda} \right) \tag{1}$$

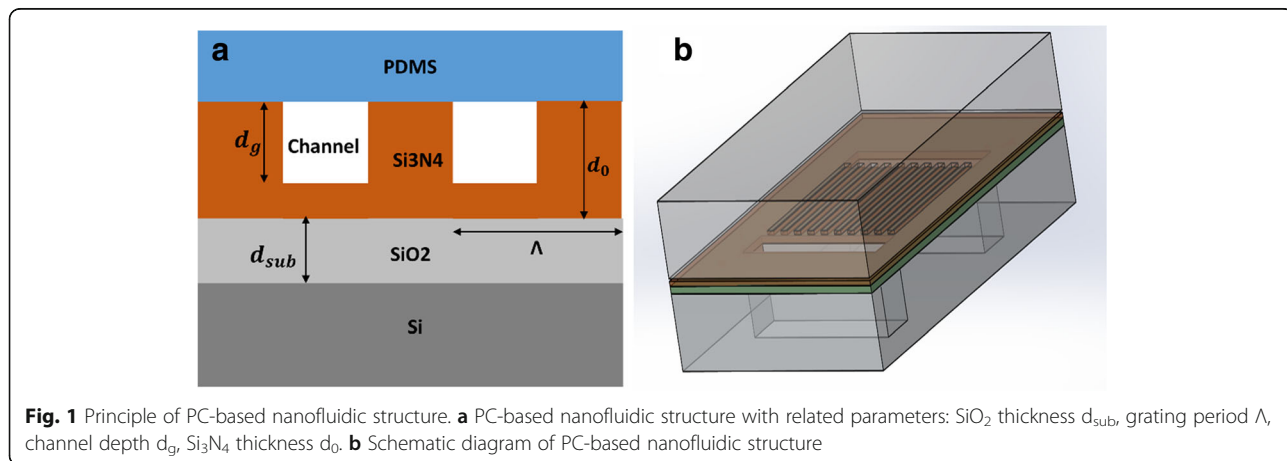
where λ is the incident light which couples into the PC, n_{eff} is the effective refractive index of photonic crystal, n_c is the refractive index of the cover layer, θ is the incident angle, and m = ±0, 1, 2... is the diffractive order. In order to simplify the structure for fabrication and experiments, the incident angle is always vertical to the surface of the PC, and the fill factor of the grating is 0.5. So, the equation can be simplified as Eq. (2):

$$\lambda = \Lambda n_{eff} \tag{2}$$

,which shows a concise relationship among resonance wavelength, PC grating pitch, and effective refractive index. The effective refractive index can be roughly regraded as weighting average refractive index of Si₃N₄, channel liquid, and PDMS.

Simulation Result and Analysis

As the shape of gratings were rectangular, the gap between PC gratings can be used to fabricate channels when the gratings’ top is sealed with PDMS. With this novelty design, the PC gratings were used as nanofluidic channel. FDTD Solutions from Lumerical Inc. had been



used for electromagnetic field simulation. Based on our former design method that had been published in [24], the parameters of PC-based nanofluidic structure had been optimized [25]. The gratings period was set as 400 nm, which is a reasonable value for PC fabrication with resonance wavelength located at visible wavelength range. The reason for fixing PC's grating period is that it is difficult to tune the pitch among fabrication processes, while it is relatively easier to vary the Si_3N_4 thickness d_0 and grating depth d_g . By tuning the Si_3N_4 thickness and grating depth, the PC resonance wavelength can be changed according to the requirements. Then, the remained parameters that need to be optimized in FDTD is the Si_3N_4 thickness d_0 and grating depth d_g . Particle swarm optimization algorithm in FDTD had been used to select the appropriate PC structure parameters.

During FDTD simulation, the incident light was a TE-polarized plane wave that ranges from 400 to 700 nm, and the direction of the incident light was perpendicular to the top surface of PC plane, as shown in Fig. 2. The fixed parameters of PC structure were grating period $\Lambda = 400$ nm, the thickness of SiO_2 substrate $d_{\text{SiO}_2} = 2$ μm , and the refractive indexes of Si_3N_4 , PDMS, and channel liquid were set as 2.02, 1.45, and 1.33, respectively. Then, the thickness of Si_3N_4 d_0 was varying as 500, 450, 400, 350, and 300 nm, while the grating depth d_g was changing as d_0 , $d_0 - 50$ nm, $d_0 - 100$ nm, ..., 100 nm, 50 nm. By using different Si_3N_4 thickness d_0 and grating depth d_g , a series of PC structure were obtained. The electric field distribution and enhancement factor of all these PC structures were obtained by running FDTD simulation software, and the PC structure which can yield an appropriate electric field distribution and enhancement factor was chosen as our sensor structure. The related PC based FDTD simulation process can be found in our former published papers [24, 26].

The final optimized results were shown as follows: PC period Λ was 400 nm, Si_3N_4 thickness d_0 was 450 nm, and grating depth d_g was 350 nm. With the grating depth located at 350 nm, most of the channel area was inside the active region of evanescent field, and the performance of PC based nanofluidic structure can be improved with this structure.

As shown in Fig. 3a, when the light source is collimated and TE polarized, the PC's spectrum has two peaks around visible range at normal incidence. The peak at 698 nm was the zero order mode TE00, and the peak at 595 nm is the first order mode TE01. In application, visible light is much easier to capture during the label-free detection. So, the first order peak was selected for label-free detection. As shown in Fig. 3b, the electric field intensity of peak at 595 nm has been obtained, and the red-dashed box represents the area in which it is used as nanochannel. It indicated that the enhanced E-field was almost confined in the channel area, which means that the electric field can interact with the sample in the channel sufficiently. The maximum electric field enhancement is more than 7 times larger than the initial incident light electric field. The former reported PC structures may have a much high maximum E-field-enhanced intensity. However, the enhanced area is usually located around the corners of the gratings or the inside part of the high refractive index layer [27, 28]. In the former structure, the enhanced E-field cannot interact with the sample thoroughly, which may degrade the performance of PC-based sensors.

Results and Discussion

Design Flow of PC-Based Nanofluidic Structure

All the experiments were accomplished on a 4-in. Si wafer, and CMOS-compatible process has been used for fabrication. As shown in Fig. 4, the designed flow of the nanofluidic sensor is as follows: (1) Si wafer clean, (2) 2 μm SiO_2 deposited on Si wafer as PC substrate, (3) 450 nm Si_3N_4

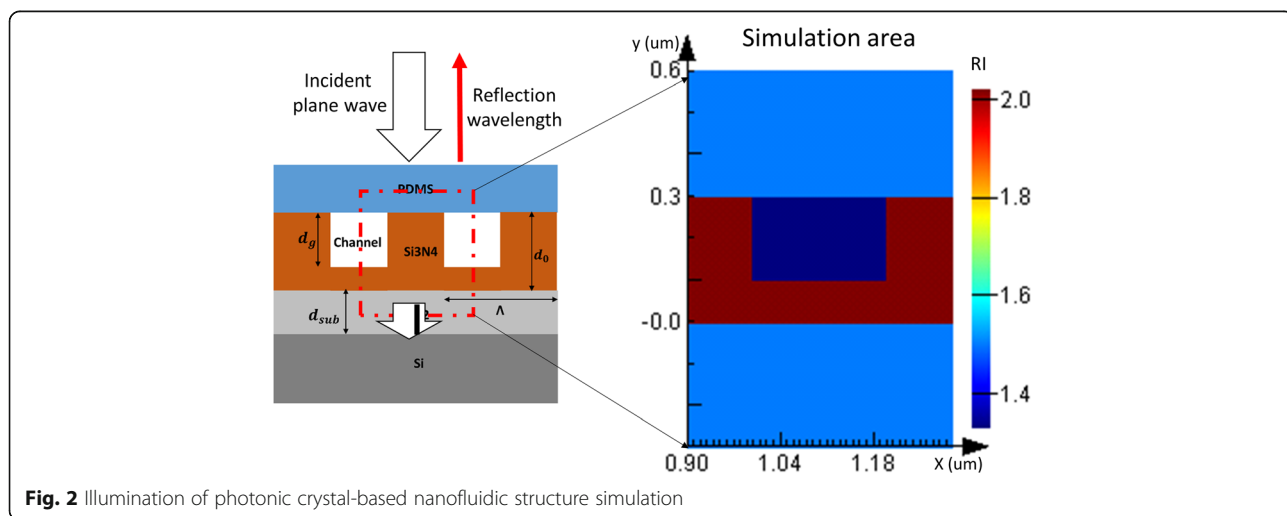


Fig. 2 Illumination of photonic crystal-based nanofluidic structure simulation

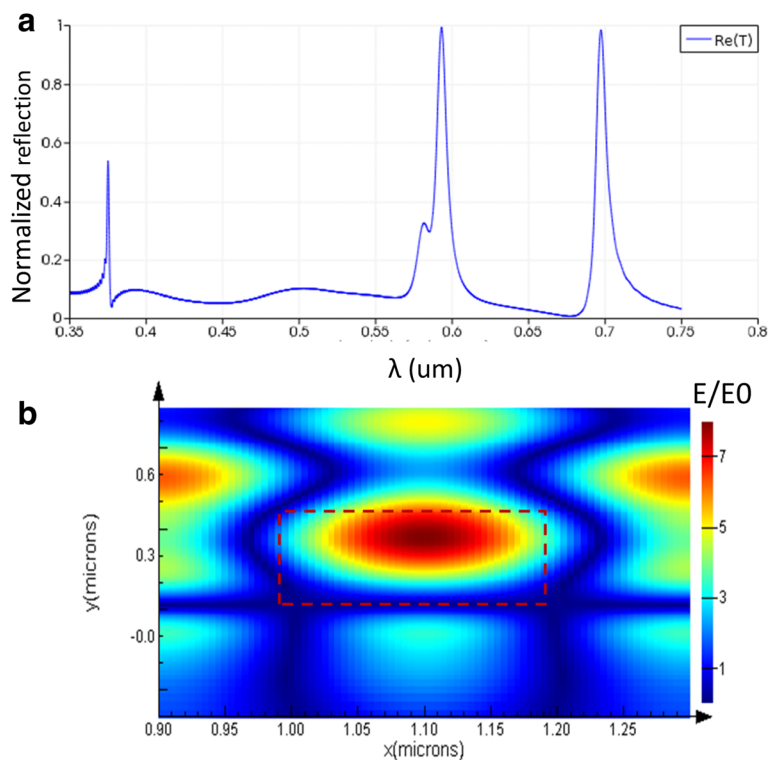


Fig. 3 Simulation result of PC-based nanofluidic structure, TE polarized, SiO_2 thickness $d_{\text{sub}} 2 \mu\text{m}$, grating period $\Lambda 400 \text{ nm}$, channel depth $d_g 350 \text{ nm}$, Si_3N_4 thickness $d_0 450 \text{ nm}$. **a** Normalized reflection spectrum of PC, peak wavelength value (PWW) at TE00 698 nm, peak wavelength value at TE01 595 nm. **b** Electrical field enhancement of PC-based nanofluidic structure with PWW at 598 nm

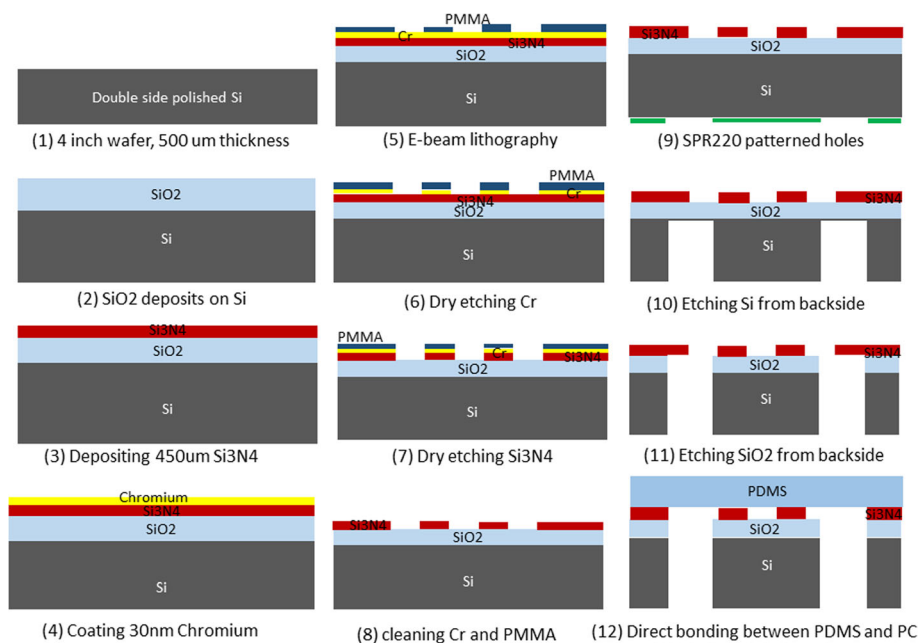


Fig. 4 Fabrication flow process of PC-based nanofluidic structure

deposited on SiO₂ layer as PC high refractive index layer, (4) 30 nm Cr coated as hard mask, (5) 2600 nm PMMA spin coated on Cr as photoresist for e-beam grating writing, (6) etching Cr layer with patterned PMMA as mask, (7) etching Si₃N₄ layer with etched Cr layer as mask, (8) removing PMMA and Cr, (9) patterned inlets/outlets from backside of the wafer with optical lithography, (10) etching through Si layer with SPR 220 as photoresist, (11) etching SiO₂ with Si as mask layer, (12) directed bonding between PDMS and patterned Si wafer.

SiO₂ and Si₃N₄ Deposition Experiments

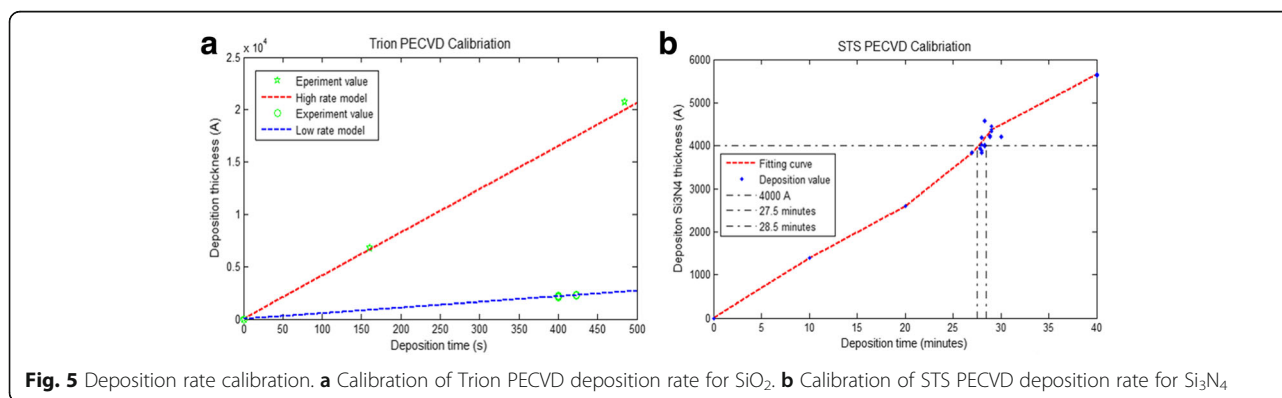
The double side polished Si wafer (100) was boron doped from Wafer World, Inc. A piranha process with 1:1 volumetric mixture of concentrated sulfuric acid (H₂SO₄) and hydrogen peroxide (wt. 30%) was used to clean the Si wafer at 60 °C for 10 min. Then, the wafer was rinsed by DI water and dried with N₂ gas. For the deposition of SiO₂, Trion PECVD (Plasma Enhanced Chemical Vapor Deposition) with high/low deposition rates were used. As shown in Fig. 5a, the high deposition rate is much faster while the film density of low deposition rate method is much higher and with less pin holes inside the SiO₂ thin film. Since the SiO₂ layer is 2 μm, the low deposition rate (320 Å/min, ±25 Å) was selected, with temperature at 350 °C, ICP power 102 W and gases of N₂O, N₂, and SiH₄.

After the deposition of SiO₂ film on Si wafer, a thickness of 450-nm Si₃N₄ film was deposited on the top of SiO₂ film as guided mode layer. Since Si₃N₄ was used as the guided layer for photonic crystal, the thickness of Si₃N₄ has a critical influence to the resonance wavelength of photonic crystal-based nanofluidic structure according to Eq. (2). In order to deposit the Si₃N₄ layer matches with the designed Si₃N₄ thickness at 450 nm, the deposition rate of Si₃N₄ was carefully calibrated. The Si₃N₄ deposition process was processed in STS PECVD. The recipe for Si₃N₄ deposition was RF frequency 13.65 MHz, power 20 W, N₂ flow rate (1960 sccm) 10%, SiH₄ flow rate (80 sccm) 20%, NH₃ flow rate (55 sccm) 10%, and chamber pressure 900 mTorr. In order to

calibrate the deposition rate of Si₃N₄, a sequence of testing experiments had been done, as shown in Fig. 5b. The result from Fig. 5b shows that the deposition rate is almost constant, about 143 Å/min.

CMOS-Compatible Fabrication Process

As Si₃N₄ is dielectric and transparent upon visible wavelength region, it is difficult to find the nano patterns with microscope. Chrome had been selected as hard mask for Si₃N₄ layer, which is much easier to pattern with Cr under e-beam equipment. The coating of 30 nm chrome was done by CHA SEC-600 e-beam Evaporator, with a coating rate of 1 Å/s under vacuum condition. Then, e-beam lithography was used for patterning nano structures on the sample wafer with PMMA. Firstly, the sample wafer was cleaned by acetone, IPA, DI water, and IPA in consequence, and then dried with N₂ gas. Then, PMMA was spun coated on the wafer as photoresist with Headway Spinner under 3000 rpm, and then preexposed on a 110 °C hot plate for 1 min. Then, the PMMA-coated wafer was patterned by the Zenith e-beam lithography equipment, and the designed grating patterns were written on the PMMA layer. Then, the patterned PMMA wafer sample was post exposure at 220 °C for 1 min and cleaned, as shown in Fig. 6a. With the PMMA patterns as mask for Cr etching, there are two etching methods: dry etching and wet etching. Dry etching was using reactive ions such as chloride ions to react with Cr as selectively etching, and also the ions physical bombardment was used to etch the surface of PMMA and Cr simultaneously. Wet etching was using Cr etchant to etch chrome, which is much faster but it would destroy the sidewall of nano patterns. As Cr was used as hard mask, dry etching method was much more stable and conformal than wet etching method, and the Cr was etched on a Plasma Thermal SLR 770 ICP RIE. As shown in Fig. 6b, c, dry etching is anisotropic, so the shape of grating is uniform, and the fidelity of grating structure is quite well, while wet etching is isotopically, and it can cause damage to the grating patterns.



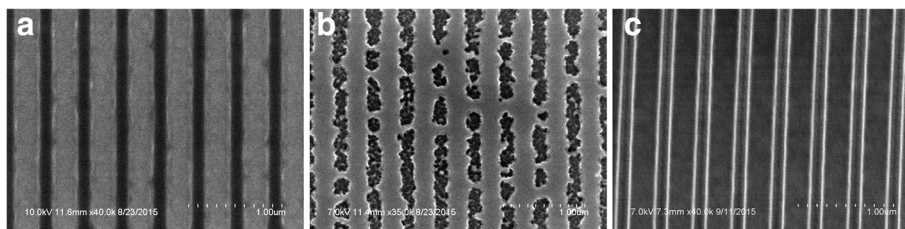
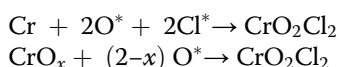


Fig. 6 SEM pictures of grating patterns. **a** E-beam-patterned grating of PMMA on top of Cr layer, **b** Wet etching Cr with Chrome etchant. **c** Dry etching Cr with STS thermal ICP RIE

The ion gas used for Cr etching was Cl_2 , Ar, and O_2 . The chemical reaction process for dry etching was as follows:



Since argon is an inertial gas, the accelerated argon gas has high momentum which can be used to bombardment of the Cr surface as physical sputtering. The recipe for chrome etching was ICP 100 W, RIE 250 W, pressure 50 mTorr, Ar 4 sccm, and O_2 6 sccm. The etch rate was about 4 nm/min. After Cr etching, the Cr pattern was used as hard mask for Si_3N_4 etching. As the etching rate between small features and buck samples was quite different, four 2 mm × 2 mm e-beam patterned samples were used for testing and calibrating. The dry etching result of Cr layer was shown in Fig. 7. The depth of the Cr layer is about 27.5 nm with grating pitch at 400 nm, and the profile of grating structures is quite uniform.

The equipment used for Si_3N_4 etching was STS Thermal Plasma ICP RIE. Since metal mask would contaminate the process chamber and it was hard to clean, this equipment was chosen specially for metal mask etching. The recipe for Si_3N_4 etching was Freon 14(CF4) 30 sccm, pressure 35 mTorr, RIE 95 W, ICP 300 W. The calibrated Si_3N_4 etching time was 4 min for 350 nm. In

order to transfer the required feature to the Si_3N_4 layer, there were two different material layers that were acting as mask, PMMA layer, and Cr layer. As the grating feature was written on the surface of PMMA by e-beam lithography, the PMMA was used as mask for Cr etching. While the grating patterns transfer to the Cr layer, the etched Cr was used as mask for Si_3N_4 etching. Moreover, with the existence of undercutting effect, it was difficult to ensure the fill factor locates at 0.5. In order to obtain the desired fill factor and structure, a sequence of six different doses was used for e-beam lithography while writing on the surface of PMMA, as shown in Fig. 8a. Then, the dose-related samples were used for Cr etching and obtained SEM grating profiles, as shown in Fig. 8b. After the related etching of Cr and Si_3N_4 layer, six different Si_3N_4 grating patterns were sculptured, as shown in Fig. 8c.

According to the fill factor calculation results, dose 1 had been selected for e-beam lithography and final experiment, and the result is shown in Fig. 9a, b. The inspected result from AFM is shown in Fig. 9a. From the AFM profile, it can be known that the grating pitch is located at 400 nm and the grating depth is about 367 nm. As the grating pitch was 400 nm with a fill factor 0.5, it was difficult for the AFM tip to touch the bottom of the grating and have a rectangular shape, so

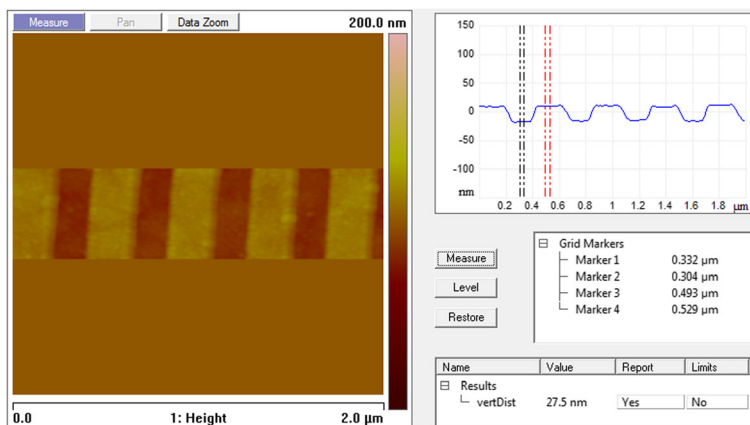


Fig. 7 AFM picture of etched Cr layer profile

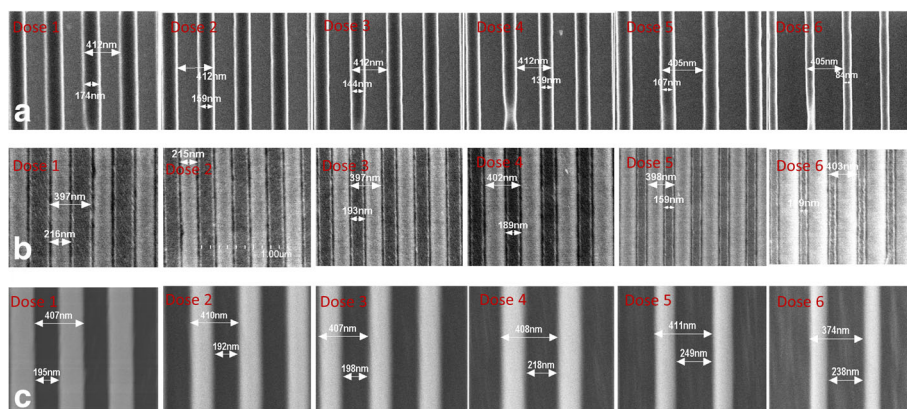


Fig. 8 SEM pictures of dose-related PC grating structures, six different e-beam lithography doses were used for fabrication. **a** PMMA gratings patterned by e-beam lithography. **b** Cr gratings with patterned PMMA as photoresist. **c** Si₃N₄ gratings as guided mode layer for PC, and etched with Cr as hard mask

the profile looks like V-shape. The grating shape was detected under SEM, as shown in Fig. 8b which indicates that the sidewall of the grating is good enough.

After the etching of Si₃N₄, the PMMA and Cr remained on the sample need to be removed. The removing process was as follows: the sample was immersed in the acetone, and ultrasonic was used to speed the dissolve, and then the sample was rinsed by acetone, IPA, DI water, and IPA in sequence. Chromium etchant from Sigma-Aldrich was used to remove remained Cr. The wet etching speed was about 40 Å per minute at room temperature. With the fabricated grating structures, the inlets and outlets of PC-based nanofluidic structure were sculptured with photolithography, backside alignment, and etching in sequence. A 5-in. ferric oxide photo mask was fabricated and been used as photomask for photolithography. The photolithography process was as follows: (1) patterned Si wafer were cleaned by piranha process and O₂ plasma for 1 min at 300 W; (2) prebake at 110 °C for 2 min; (3) cooling 30 s on the cooling plate; (4) descum with O₂ plasma at 250 W, 150 mTorr for 1 min, (5) spin coating HMDS and

SPR-220 in sequence at 3000 rpm for 30 s respectively, and the thickness of the SPR-220 will be 5 um; (6) soft bake at 60 °C for 2 min and 110 °C for 1 min; (7) backside alignment and exposure with i-line photolithography from EVG 620 aligner. The photolithography dose was 180 mJ/cm² with vacuum contact and 50 μm separation distance, (8) 1:5 mixture of AZ 400 K and DI water as developer for exposed SPR-220; (9) the wafer was cleaned by DI water and N₂ gas. With the SPR-220 patterns on the back of the patterned wafer, the inlets and outlets were fabricated by etch through the Si and SiO₂ from the SPR-220 patterned side of Si wafer.

The equipment used for Si etching was STS Pegasus ICP-DRIE, which has an etch rate of 20 μm/min with Bosch process. The whole Si layer etching process took 25 min, and the etching process would stop when the etching gases met the SiO₂ layer. The etched Si pattern was used for SiO₂ etching. Plasma Therm SLR-770 ICP RIE was used for the etching process, and the calibrated SiO₂ etch rate was shown as in Fig. 10. The recipe used for SiO₂ etching was CF₄ 30 sccm, Ar 4 sccm, O₂ 5 sccm,

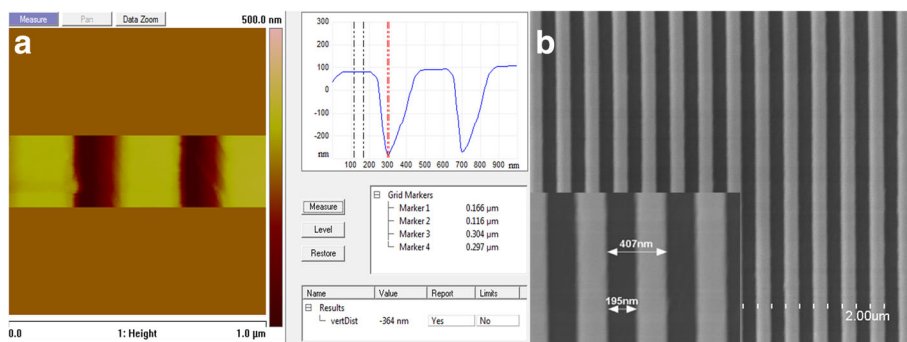


Fig. 9 Inspection profile of Si₃N₄ gratings. **a** AFM image of Si₃N₄ grating depth and profile. **b** SEM image of Si₃N₄ gratings with periodic at 400 nm and fill factor 0.5

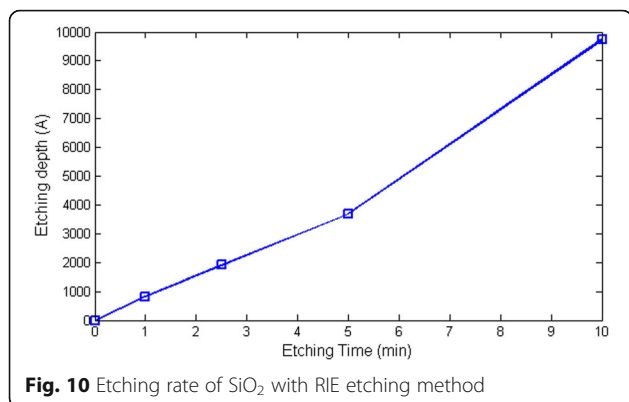


Fig. 10 Etching rate of SiO_2 with RIE etching method

RIE 250 W, ICP 50 W, and pressure 30 mTorr. The RIE power was mainly used to break the chemical bond, while ICP power was aimed to enhance the plasma density.

In order to fabricate the nanofluidic channel, a cladding layer was used to bond with the PC grating structure. Buck polydimethylsiloxane (PMDS) was made by mixing liquid PDMS and cross-linking agent. PDMS is a typical bonding method for polymer bonding, especially for rapid prototyping and used as plastic substrate. The buck PDMS and grating structure were treated with O_2 plasma (300 W, 30 s) to make the surface hydrophilic. After the surface treatment, they were directly bonded with each other as shown in Fig. 11.

Discussion

As PC's grating period Λ , grating depth d_g , and fill factor are important parameters to the final performance of PC-based nanofluidic sensor, maintaining the fabricated results conform to the designed structure parameters is of key importance. In this work, in order to keep the fabricated PC structure conform with the designed parameters, Si_3N_4 and SiO_2 deposition rates had been calibrated and deposition thicknesses were carefully controlled. The



Fig. 11 Prototype of PC-based nanofluidic structure

obtained Si_3N_4 grating thickness is 364 nm which is very close to the designed d_g 350 nm, as shown in Fig. 9. Also, the measured PC grating period Λ 400 nm, which is equal to the designed grating period, as indicated from Fig. 7. To fabricate a uniform grating structure with fill factor 0.5, six different dose of e-beam process were used, and a uniform PC grating structure was yield according to the dose 2 process. A direct bonding method was used to realize nanofluidic channels between PC grating grooves and PDMS cladding layer. The bonding process is low cost and easy to implement, which is much convenient than traditional anodic bonding process.

This kind of structure is an improvement while contrast with PC-based microfluidic sensors, basically there are two kinds of applications: (1) Concentration detection: the reflected resonance wavelength of PC-based nanofluidic sensor will shift as the concentration of the liquid sample varies. There are a lot of applications, such as alcohol concentration detection, special protein concentration detection, small molecules, and even single molecule. It can be used for medical and industry applications. (2) Fluorescence enhancement: the enhanced electric field will improve the fluorescence efficiency when the incident light matches with the exciting wavelength range of the fluorescence dye. Since plenty of biological and medical applications are fluorescence based, the fluorescence enhancement can be used to improve the limit of detection for fluorescence-based experiments. The advantages of PC-based nanofluidic sensor have two basic aspects: (1) the volume of required sample is reduced to nanoscale, which can improve the efficiency of sample dose. (2) The nanofluidic channel can guarantee the detection area be confined around the evanescent region of PC structure, which can improve the sensor's sensitivity. The function range of evanescent field is less than 400 nm, and it is the main region of enhanced electric field, which will interact with the fluid sample and obtain a resonance wavelength shift. With these unique performances, the PC-based nanofluidic structure sensor can be used for biomedical, chemical, and even clinic application applications in the near future.

Conclusions

CMOS-compatible process of PC-based nanofluidic structure had been proposed, designed, and fabricated. The nanochannels have been created by polymer bonding between periodic gratings in PC and PDMS substrate. A detailed fabrication flow process was designed to guide the top-down fabrication process, and CMOS-compatible techniques had been used to realize the structure. The PC-based nanofluidic structure, with Si_3N_4 as its guided mode layer and SiO_2 as its substrate, has a grating period Λ 400 nm, Si_3N_4 thickness d_0 450 nm, and grating depth d_g 350 nm. The resonance wavelength at 598 nm for

higher order TE mode was selected for potential label-free detection. It is the first time that a PC-based nanofluidic structure has been proposed and realized with CMOS-compatible process. The enhanced electric field is located in the center area of nanochannels, which can be further benefit for analytes interaction experiments.

Abbreviations

CMOS: Complementary metal oxide semiconductors; DI water: Deionized water; FDTD: Finite difference time domain; IPA: Isopropyl alcohol; PC: Photonic crystal; PDMS: Polydimethylsiloxane; PWW: Peak wavelength value

Acknowledgements

This work was supported by the China Scholarship Council (No. 201306160029). WP also acknowledge the support from Professor Brian T. Cunningham and his Nano Sensors Group. Also thanks for the support from Flexible Electronics Research Center of HUST.

Authors' contributions

WP has made substantial contributions to the design, simulation, and fabrication of CMOS-compatible PC-based nanofluidic structure. Prof. YC, Prof. WA, and Prof. DZ have participated in the critical discussion of the contents and drafting of the manuscript for publication. HS, HX, and PH have revised the manuscript. All authors read and approved the final manuscript.

Competing interests

The authors declare that they have no competing interests.

Author details

¹School of Mechanical Science and Engineering, Huazhong University of Science and Technology, Wuhan 430074, China. ²Department of Electrical and Computer Engineering, University of Illinois at Urbana-Champaign, Urbana, Illinois 61801, USA. ³Micro and Nanotechnology Laboratory, University of Illinois at Urbana-Champaign, Urbana, Illinois 61801, USA. ⁴School of Mechanical and Electronic Engineering, Wuhan University of Technology, Wuhan 430070, China. ⁵Flexible Electronics Research Center, Huazhong University of Science and Technology, Wuhan 430074, China.

Received: 17 October 2016 Accepted: 13 January 2017

Published online: 09 February 2017

References

- Yablonovitch E (1987) Inhibited spontaneous emission in solid-state physics and electronics [J]. *Phys Rev Lett* 58(20):2059
- Vlasov YA, O'Boyle M, Hamann HF et al (2005) Active control of slow light on a chip with photonic crystal waveguides[J]. *Nature* 438(7064):65–69
- Knight JC, Arriaga J, Birks TA et al (2000) Anomalous dispersion in photonic crystal fiber[J]. *IEEE Photon Technol Lett* 12(7):807–809
- Zeng L, Bermel P, Yi Y et al (2008) Demonstration of enhanced absorption in thin film Si solar cells with textured photonic crystal back reflector [J]. *Appl Phys Lett* 93(22):221105
- Ge HL, Xu C, Xu K et al (2015) Enhanced performance of photonic crystal GaN light-emitting diodes with graphene transparent electrodes[J]. *Nanoscale Res Lett* 10(1):103
- Chan LL, Gosangari SL, Watkin KL et al (2007) A label-free photonic crystal biosensor imaging method for detection of cancer cell cytotoxicity and proliferation [J]. *Apoptosis* 12(6):1061–1068
- Lee MR, Fauchet PM (2007) Two-dimensional silicon photonic crystal based biosensing platform for protein detection [J]. *Opt Express* 15(8):4530–4535
- Huang CS, George S, Lu M et al (2011) Application of photonic crystal enhanced fluorescence to cancer biomarker microarrays [J]. *Anal Chem* 83(4):1425–1430
- Ganesh N, Mathias PC, Zhang W et al (2008) Distance dependence of fluorescence enhancement from photonic crystal surfaces [J]. *J Appl Phys* 103(8):083104
- Boiko V, Dovbeshko G, Dolgov L et al (2015) Angular shaping of fluorescence from synthetic opal-based photonic crystal[J]. *Nanoscale Res Lett* 10(1):1
- Chen W, Long KD, Yu H et al (2014) Enhanced live cell imaging via photonic crystal enhanced fluorescence microscopy [J]. *Analyst* 139(22):5954–5963
- Guo Y, Ye JY, Divin C et al (2010) Real-time biomolecular binding detection using a sensitive photonic crystal biosensor[J]. *Anal Chem* 82(12):5211–5218
- Konopsky VN, Alieva EV (2007) Photonic crystal surface waves for optical biosensors [J]. *Anal Chem* 79(12):4729–4735
- Monat C, Domachuk P, Eggleton BJ (2007) Integrated optofluidics: a new river of light [J]. *Nat Photonics* 1(2):106–114
- Choi CJ, Cunningham BT (2006) Single-step fabrication and characterization of photonic crystal biosensors with polymer microfluidic channels [J]. *Lab Chip* 6(10):1373–1380
- Zhang M, Peh J, Hergenrother PJ et al (2014) Detection of protein–small molecule binding using a self-referencing external cavity laser biosensor[J]. *J Am Chem Soc* 136(16):5840–5843
- Liu L, Wang B, Sha J et al (2013) Voltage-driven translocation behaviors of IgG molecule through nanopore arrays [J]. *Nanoscale Res Lett* 8(1):1–7
- Wu S, Lin Q, Yuen Y et al (2001) MEMS flow sensors for nano-fluidic applications [J]. *Sensors Actuators A Phys* 89(1):152–158
- Yanik AA, Huang M, Artar A et al (2010) Integrated nanoplasmonic-nanofluidic biosensors with targeted delivery of analytes [J]. *Appl Phys Lett* 96(2):021101
- Huang M, Yanik AA, Chang TY et al (2009) Sub-wavelength nanofluidics in photonic crystal sensors[J]. *Opt Express* 17(26):24224–24233
- Meng L, Gao J, He X et al (2015) CMOS-compatible top-down fabrication of periodic SiO₂ nanostructures using a single mask[J]. *Nanoscale Res Lett* 10(1):1–7
- Liu J-N et al (2011) Optimally designed narrowband guided-mode resonance reflectance filters for mid-infrared spectroscopy. *Opt Express* 19(24):24182–24197
- Fan S, Joannopoulos JD (2002) Analysis of guided resonances in photonic crystal slabs. [J]. *Phys Rev B* 65(23):235112
- Peng W, Chen Y, Ai W (2017) Higher-order mode photonic crystal based nanofluidic sensor [J]. *Opt Commun* 382:105–112
- The refractive index database. <http://refractiveindex.info>
- Peng W, Chen Y, Ai W et al (2016) A nanofluidic biosensor based on nanoreplica molding photonic crystal [J]. *Nanoscale Res Lett* 11(1):427
- Shamah SM, Cunningham BT (2011) Label-free cell-based assays using photonic crystal optical biosensors [J]. *Analyst* 136(6):1090–1102
- Choi CJ, Block ID, Bole B et al (2009) Label-free photonic crystal biosensor integrated microfluidic chip for determination of kinetic reaction rate constants [J]. *IEEE Sensors J* 9(12):1697–1704

Submit your manuscript to a SpringerOpen® journal and benefit from:

- Convenient online submission
- Rigorous peer review
- Immediate publication on acceptance
- Open access: articles freely available online
- High visibility within the field
- Retaining the copyright to your article

Submit your next manuscript at ► springeropen.com